Resistance Spot Welding: A Heat Transfer Study

Real and simulated welds were used to develop a model for predicting temperature distribution

BY Z. HAN, J. OROZCO, J. E. INDACOCHEA AND C. H. CHEN

ABSTRACT. A heat transfer study of resistance spot welding has been conducted both theoretically and experimentally. A numerical solution based on a finite difference formulation of the heat equation has been developed to predict temperature distributions as a function of both time and position during the welding process. The computer model also predicts the temperature distribution through the copper electrodes. One important feature of the program is that it allows for variations in the physical properties of the metal workpiece.

Temperature measurements have been made in real and simulated welds of a high-strength low-alloy (HSLA) sheet steel. Excellent agreement is obtained between the numerical solution and the experimental measurements. The heat-affected zone (HAZ) obtained by plotting the lines of constant temperature is very similar to that measured from actual welds.

Introduction

Resistance spot welding is characterized as a rapid and clean process for joining sheet steel. Despite its long and wide commercial application, an adequate weld nugget size is still the primary concern for spot welding qualification procedures (Refs. 1, 2). Weld nugget sizes have been estimated conventionally, using a number of destructive tests, and recently using more sophisticated techniques, such as ultrasonic and dynamic resistivity profiles (Refs. 3-5). However, it has been pointed out by other investigators (Ref. 6) that seldom has the nugget size been directly and methodically correlated with the different welding process parameters.

KEY WORDS

Resistance Spot Weld
Spot Welding
HSLA Steels
Heat Transfer Model
Temperature Spread
Copper Electrodes
Nugget Size
Heat Conduction
Heat of Fusion
Computer Model

Z. HAN, J. OROZCO and J. E. INDACOCHEA are with the University of Illinois at Chicago, Chicago, Ill. C. H. CHEN is with Inland Steel Laboratories, East Chicago, Ind.

A survey of the literature on resistance welding (Refs. 7-11) reveals that most of the thermal models currently available to describe the resistance spot welding process are either too basic (one-dimensional) or do not include some of the fundamental variables. For instance, the variation of contact resistance with applied electrode force is not included in the heat transfer formulation, nor is it the effect of temperature on physical properties of the material.

This investigation has been undertaken to address some of these issues. Basically, in this work a heat transfer model is proposed for predicting the temperature as a function of time, from the start of the weld, and as a function of position, for any location within the weld nugget, adjacent heat-affected regions or electrodes. This heat transfer model takes into account the following considerations: conduction in the solid, convection, heat of fusion due to solid-liquid phase change, element heat content as a function of time and temperature, conduction in the weld pool, and heat of fusion on resolidification.

For the analysis of the temperature distribution in the sheet metal, it is known that there is a symmetrical distribution of temperatures through the thickness of the material and along the interface where the two sheet pieces meet. Consequently, a cylindrical coordinate system was selected (Fig. 1) with radial as well as vertical variations in temperature and the assumption of azimuthal symmetry in ϕ. The basic equations and the corresponding boundary conditions are expressed in finite difference forms. The solution to the equations includes an explicit formulation which incorporates the physical properties of the HSLA (high-strength low-alloy) sheet steel, the base metal.

The analytical thermal results have been correlated with the information obtained from real and simulated weld heat-affected zones (HAZ). The real resistance spot welds were processed at the Inland Steel Research Laboratories, while the simulated weld HAZ's were produced at the University of Illinois at Chicago Welding and Joining Laboratories. The temperature computations were performed for different power levels, several welding efficiencies, various electrode forces and corresponding material contact resistances. The model also accounts for the temperature dependence of the physical properties of the base metal.

Physical and Mathematical Formulation

The weld nugget in resistance spot welding is produced by the melting and subsequent coalescence of a small volume of material due to the heating caused by the passage of the electric current and the high contact resistance between the sheet metals joined. Such heating per unit time (Q) is defined as the product of the current intensity (I) squared, times the total resistance (R), times the welding efficiency (η).

Several authors (Refs. 12-14) have reported continuous variations in the electrical parameters during welding of mild steel sheet. After about the first cycle, there is an increase in voltage across the copper electrodes and a reduction in current flowing through the weld zone until a "peak state" is reached. Throughout the remaining portion of the weld cycle, the voltage decreases to a constant value while the current increases also to a constant value. These changes in voltage and current have also been represented as dynamic resistance (Refs. 12-14). Basic welding mechanisms

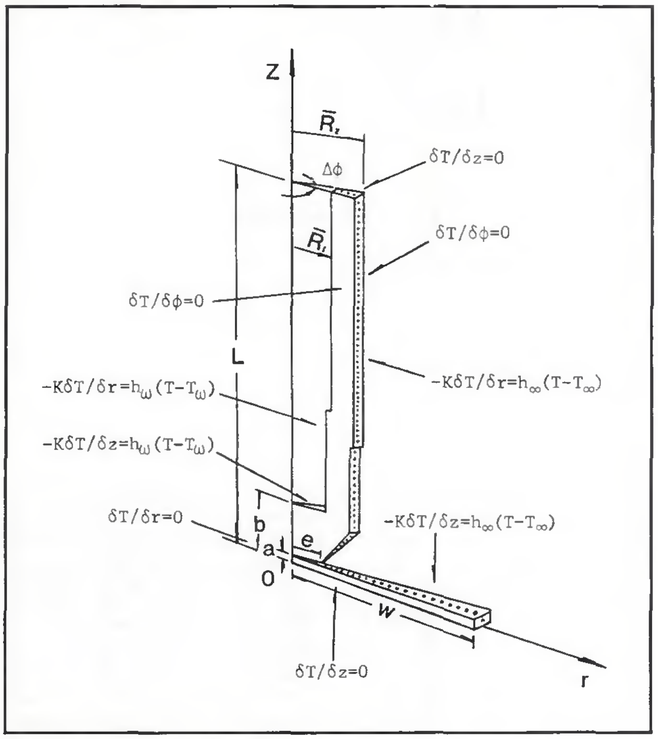

Fig. 1—Schematic describing thermal boundary conditions

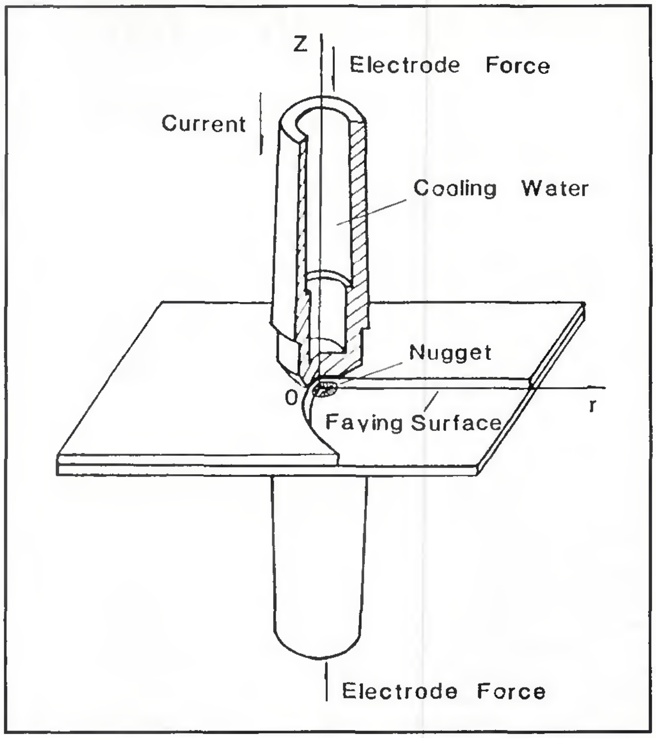

Fig. 2—Schematic of the resistance spot welding process

can be altered by changes in welding variables such as weld time, electrode force and overall weld current.

The components of the system for resistance spot welding are schematically represented in Fig. 2. The copper electrodes are water cooled; they exert a concentrated force on the outer surfaces of the metals to be joined. Because of their low electric resistance, these electrodes can conduct high currents to the workpiece without significant Joule heating losses. Further, their high thermal conductivity permits closer control of the nugget formation as well as the cooling rate, by conducting heat away from the workpiece (Ref. 15).

The resistances of the sheet steels to be joined are relatively small, so that a large current flow is needed to produce a high-Joule heating effect in the workpiece. The largest voltage drop occurs in the workpiece, because the resistivity of the copper electrodes is an order of magnitude lower than that of the carbon steel (Ref. 16). This generates the highest internal heat production in the workpiece, and melting takes place at the common interface of the workpiece and spreads to produce the weld nugget. This phase change from solid to liquid will cause a drastic change in the physical properties of the sheet steel.

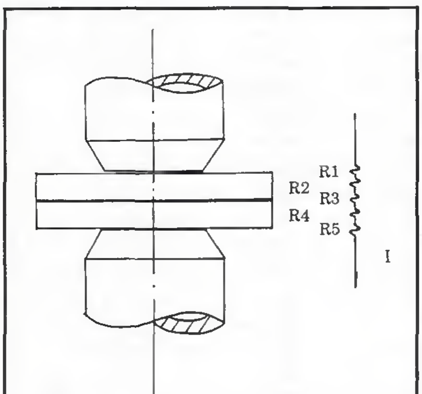

Fig. 3—Simplification of the resistance across the electrodes

The total resistance across the electrodes could be considered as the sum of five resistors in the series schematically represented in Fig. 3. R_1 and R_5 are the interface resistances between the electrodes and the sheet metal; R_2 and R_4 represent the metals' bulk resistance. R_3 is defined as the contact resistance at the faying interface and is affected by the electrical, mechanical and thermal condition of the surface. Since melting occurs at this last interface, heat production is the greatest at this location, implying that R_3 is much larger than the other resistances. However, this value drops to zero (Appendix A) as the weld nugget is formed.

Model Assumptions

In modeling the resistance spot welding process, several boundary conditions and physical phenomena must be considered. In simplifying this thermal model, the following assumptions are made:

1) A cylindrical coordinate system was selected as illustrated in Fig. 1. The portions of the coupon affected by the heat and the immediate-adjacent areas of the unaffected base metal have been represented by a disk of radius ω (ω = 25 mm), because of the temperature symmetry. This selection reduces the geometrical dependency to two dimensions, hence

$$T = T(r,z,\phi) \quad (1)$$

2) The temperature of the inner surface of the electrodes is that of the cooling water, T_w.

3) Natural convection is the dominant mechanism on the outer surface of the electrodes as well as on the surface of the workpiece.

4) Symmetry with respect to ϕ, the azimuthal angle, permits heat transfer in the radial and vertical directions only. The boundary conditions created by symmetry are indicated in Fig. 1.

5) The materials are subjected to a wide range of temperatures. Properties such as thermal conductivity (K), thermal diffusivity (α), specific heat (C_p) and resistivity (ρ) must then be considered as functions of temperatures. For our study, the thermal properties considered were those of low-carbon steel, as shown in Fig. 4 (Refs. 14, 16-19). Equations have been developed for these properties as function of temperature from the data in Fig. 4.

The thermal conductivity is expressed as:

$$K = K_o[1 - 0.0004528(T - 20)] \quad (2)$$

where

$K_o = 5.4 \times 10^7$ erg/s · mm · °C

The equations for the specific heat were derived taking into consideration four temperature ranges as noted below

(i) $T \leq 520°C$,

$$C_p = C_{p_o} [1 + 0.000688(T - 20)] \quad (3)$$

and

$$C_{p_o} = 4.65 \times 10^8 \text{ erg/g} \cdot °C$$

(ii) $520°C < T \leq 770°C$,

$$C_p = C_{p_o} \cdot T^4 \quad (4)$$

and

$$C_{p_o} = 8.55 \times 10^3 \text{ erg/g} \cdot °C$$

(iii) $770°C < T \leq 850°C$,

$$C_p = C_{p_o}(T - 850)^4 + 7.118 \times 10^8 \quad (5)$$

and

$$C_{p_o} = 13.716 \text{ erg/g} \cdot °C$$

(iv) $T > 850°C$

$$C_p = 6.25 \times 10^8 \text{ erg/g} \cdot °C \quad (6)$$

The equation developed for the resistivity is:

$$\rho = \rho_o[1 + 0.005(T - 20)] \quad (7)$$

and

$$\rho_o = 1.5 \ \mu\Omega\text{-mm}$$

6) The contact resistance at the faying interface varies with electrode force as shown in Fig. 4D (Ref. 14). At relatively low electrode forces, this resistance is so large that the bulk resistance of the sheet metal is neglected. The empirical equation that was derived from the information provided by Fig. 4D for the low-carbon steel is:

$$\rho' = \rho'_o (1 - 0.0004754 \text{ P}) \quad (8)$$

$$\rho'_o = 15 \ \mu\Omega\text{-mm}$$

where P is the electrode force on the workpiece in units of pounds.

7) Since the tip surfaces of the copper electrodes are not only easily deformed, but also polished before welding, the electrode/sheet metal interface resistances, R_1 and R_5, are assumed to be negligible.

8) Since the metal undergoes a phase change, a latent heat of fusion evolves which is assumed to be isothermally absorbed.

9) The initial temperature of the metal is the ambient temperature, T_∞.

Mathematical Model

Governing Differential Equation and Conditions

The three-dimensional heat conduction equation is written in cylindrical coordinates at an inner node as follows

$$\rho''C_p \ \partial T/\partial t = (1/r)[\partial/\partial r(rK\partial T/\partial r)] + (K/r^2)(\partial^2 T/\partial \phi^2) + K(\partial^2 T/\partial z^2) + g \quad (9)$$

where ρ'' is the density of the steel sheet or copper electrode, and g is the heat contribution due to the Joule heating effect. However, since the system is symmetrical with respect to ϕ as assumed in the model assumptions

$$\partial^2 T/\partial \phi^2 = 0 \quad (10)$$

The initial temperature of the system is that of the ambient, thus

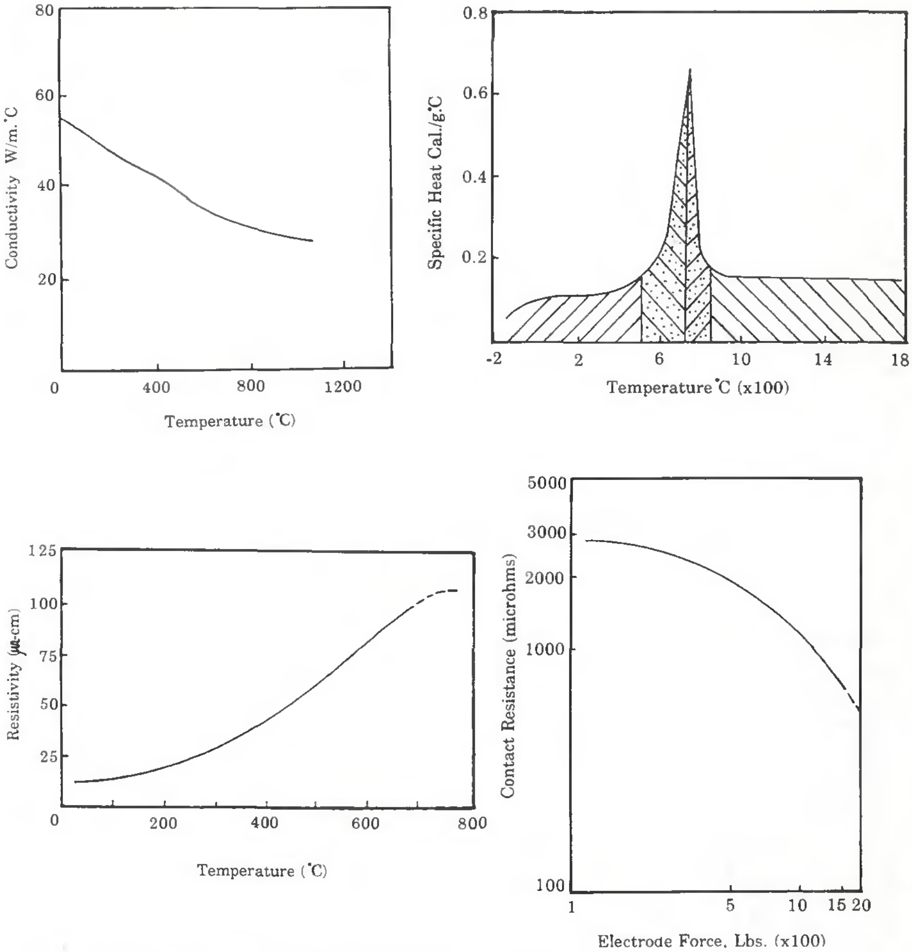

Fig. 4—Physical properties of low-carbon steels of conductivity, specific heat, bulk resistivity and contact resistance as a function of temperature and electrode force (Refs. 14, 16–19)

$$T(r,z,t_o) = T_\infty \quad \text{(constant)} \quad (11)$$

The adiabatic boundary conditions on the workpiece, as shown in Fig. 1, are

$$\partial T/\partial r = 0 \text{ at } r = 0 \text{ for } 0 \leq z \leq b \quad (12)$$

$$\partial T/\partial z = 0 \text{ at } z = L \text{ for } \bar{R}_1 \leq r \leq \bar{R}_2 \quad (13)$$

$$\partial T/\partial \phi = 0 \text{ everywhere} \quad (14)$$

The convective boundary conditions on the workpiece are

$$-K\partial T/\partial r = h_\infty (T - T_\infty) \text{ at } r = w \text{ for } 0 \leq z \leq a \quad (15)$$

$$-K\partial T/\partial z = h_\infty (T - T_\infty) \text{ at } z = a \text{ for } e \leq r \leq w \quad (16)$$

The boundary conditions on the electrode are

$$-K\partial T/\partial r = h_\infty(T - T_\infty) \text{ along the outer surface of the electrode} \quad (17)$$

$$-K\partial T/\partial r = h_w(T - T_w) \text{ along the inner surface} \quad (18)$$

All the boundary conditions are identified in Fig. 1.

Finite Difference Representation of the Heat Equation

Attention is now focused on the mesh shown in Fig. 5. The first and second derivatives of the temperature with respect to position at a point i, j may be written as

$$\left.\frac{\partial T}{\partial r}\right|_{i,j,n} = (T^n_{i+\frac{1}{2},j} - T^n_{i-\frac{1}{2},j})/\ell \quad (19)$$

$$\left.\frac{\partial^2 T}{\partial r^2}\right|_{i,j,n} = (T^n_{i+1,j} + T^n_{i-1,j} - 2T^n_{i,j})/\ell^2 \quad (20)$$

$$\left.\frac{\partial^2 T}{\partial z^2}\right|_{i,j,n} = (T^n_{i,j+1} + T^n_{i,j-1} - 2T^n_{i,j})/\ell^2 \quad (21)$$

The derivative of temperature for a node i, j with respect to time is written as

$$\left.\frac{\partial T}{\partial t}\right|_{i,j,n} = (T^{n+1}_{i,j} - T^n_{i,j})/\Delta t \quad (22)$$

where i, j and n are integers.

Equation 10 and Equations 19 through 22 are now substituted into Equation 9 to yield

$$\frac{1}{\ell^2}\left[\begin{array}{c} T^n_{i+1,j} + T^n_{i-1,j} + \\ T^n_{i,j+1} + T^n_{i,j-1} - 4T^n_{i,j} \end{array}\right] + \frac{g^n_{i,j}}{K} = \frac{1}{\alpha}\left[\frac{T^{n+1}_{i,j} - T^n_{i,j}}{\Delta t}\right] \quad (23)$$

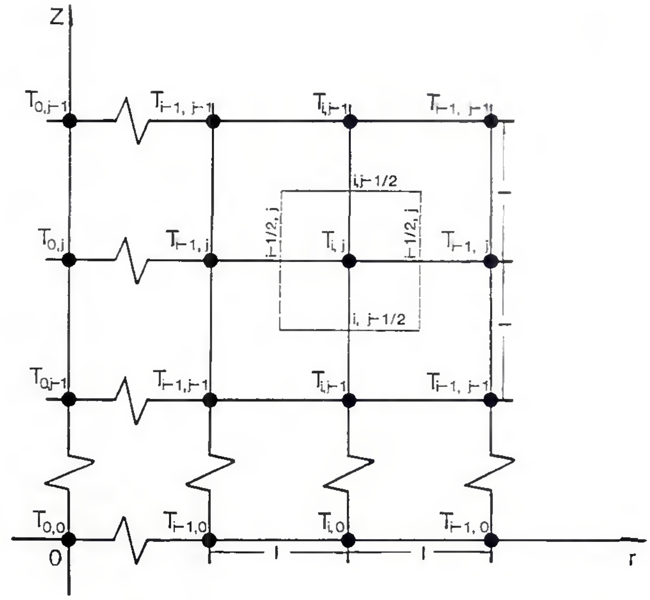

Fig. 5 — Rectangular net mesh of size 1 and a node (i,j) inside the matrix

where $g^n_{i,j}$ is the energy generation term at node i,j and moment n. Applying the above formulation to those nodes on boundaries, we can develop a general expression to obtain the temperature value at any node i,j and moment n + 1 as follows

$$T^{n+1}_{i,j} = \frac{K\Delta t}{\rho'' C_p \ell^2}\left[T^n_{i+1,j} + T^n_{i-1,j} + T^n_{i,j+1} + T^n_{i,j-1}\right] + \frac{\Delta t}{\rho'' C_p} g^n_{i,j} + \left[1 - \frac{4K\Delta t}{\rho'' C_p \ell^2}\right] T^n_{i,j} + q^n_{i,j} \qquad (24)$$

where $q^n_{i,j}$ is related to convective process. If node i, j is located within the system or on adiabatic boundaries, then

$$q^n_{i,j} = 0$$

$$g^n_{i,j} \begin{cases} >0 & \text{for } 0 \leq i \leq 4,\ 0 \leq j \leq 2 \\ = 0 & \text{everywhere else} \end{cases} \qquad (25)$$

for node i, j located on outer surface, we have

$$q^n_{i,j} = \frac{\Delta t\, h_\infty}{\rho'' C_p \ell}(T^n_{i,j} - T_\infty) \qquad (26)$$

$$g^n_{i,j} = 0$$

and finally, for node i, j located on the inner surface of the electrodes, we have

$$q^n_{i,j} = \frac{\Delta t\, h_w}{\rho'' C_p \ell}(T^n_{i,j} - T_w) \qquad (27)$$

$$g^n_{i,j} = 0$$

At the origin, r = 0, Equation 9 would have a singularity because as r approaches zero $(1/r)(\partial T/\partial r)$ would be undefined. To deal with this situation, we have that for r = 0

$$\lim_{r \to 0} [(1/r)(\partial T/\partial r)] = \partial^2 T/\partial r^2 \qquad (28)$$

then the heat-conduction Equation 9 at the location r = 0 takes the form

$$2\partial^2 T/\partial r^2 + \partial^2 T/\partial z^2 + (1/K)g = (1/\alpha)\partial T/\partial t \qquad (29)$$

similar formulations are also developed for points along the boundaries. However, for simplicity their development is omitted.

Numerical Method

The governing differential equation was written in finite difference form and solved using an explicit method. The explicit method is relatively straightforward but requires a large amount of computing time because of the stringent stability condition which is expressed as $\Delta t < (\rho'' C_p/2\Delta r)^2/[1 + (\Delta r)^2/(r\Delta t)^2]$. In this study, the minimum time step used is 0.00015 s.

Experimental Procedures

A cold-rolled HSLA sheet steel, 2.18 mm (0.086 in.) thick was used in this investigation. Its composition is given in Table 1. The material was cut to small coupons of dimensions of 101.6 × 25.4 mm (4.0 × 1.0 in.). The surfaces of the specimens were previously cleaned with acetone. The spot welds were produced by placing two specimens into a special welding fixture — Fig. 6. The fixture attaches to the lower copper electrode.

The spot welding was done on a Sciaky press-type 100-kVA single-phase resistance welding machine. The electrode force on welding was 1600 lbf (7120 N). The electrodes used were a Class II copper alloy (99.2% Cu, 0.8% Cr) based on the Resistance Welder Manufacturers' Association (RWMA) standard. The electrode tips have a contact diameter of 7.9 mm (0.31 in.) and 45-deg truncated cone nose in accordance to the Ford Motor Company manufacturing standards. The welding time was held fixed at 23 cycles (0.38 s) and the current varied between 11 and 12 kA.

The thermal cycle measurements during resistance welding were measured by spot welding a 0.254-mm (0.010-in.) thermocouple (either a chromel/alumel or a platinum/platinum-10% rhodium) onto a 0.8–1.1-mm (0.032–0.045-in.) wide slot machined on the upper coupon as shown in Fig. 7. The slot was machined so as to end in the HAZ, and its length was estimated by performing a metallographic analysis on several preliminary spot welds. The welds were sectioned through the nugget normal to the plane

Fig. 6 — Welding fixture used for production of spot welds

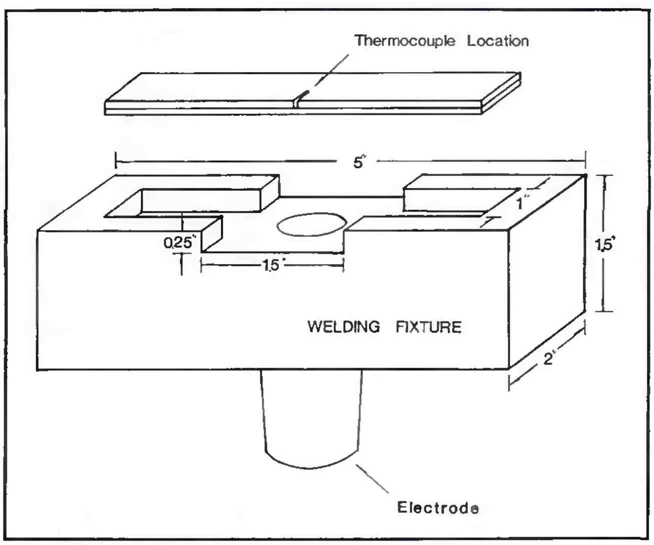

of the sheet. Samples were mechanically polished and etched with a solution of picric acid plus sodium tridecylbenzene sulfonate. This etchant was very effective in revealing the solidification structure of the weld nugget. Samples were characterized with a Leco 300 metallograph. The nugget size, as well as HAZ measurements, were made from the resulting micrographs and Fig. 8 shows one of several photo composites that were assembled for the metallographic analyses. The HAZ was observed to be the widest at the faying interface. The thermocouples were placed very close to this faying surface, and its exact location was later determined by metallographic evaluation after welding. The thermal measurements were collected using a Hewlett-Packard Series 3000 personal computer with a 3852 data acquisition unit and a Xerox 6060 personal computer interphased with a metrobyte data acquisition system. The thermocouple output signal was distorted during the heating cycle, but then it remained very smooth during cooling, immediately after the end of the weld cycle. The peak temperature was obtained by extrapolating the cooling curve to a time coinciding with the end of the weld time.

Results and Discussion

The heat transfer model developed in this study includes in its formulation the independent process parameters such as current, electrode force and time, the material's thermally dependent physical properties and the weld efficiency factor. The analytical results predicted by the model are compared with those obtained experimentally.

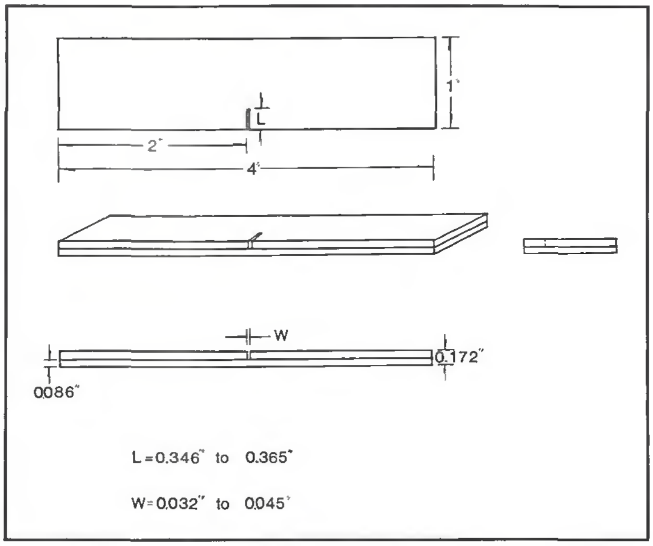

Fig. 7—Sheet steel coupons for the spot welds

Table 1—Composition of the HSLA-Sheet Steel wt-%

C	Mn	Si	Nb	Ti	Al	N	S	P
0.06	0.96	0.03	0.10	0.002	0.060	0.006	0.012	0.009

Effect of Current Level on Nugget Formation

Automotive companies' spot weld qualification procedures (Refs. 1, 2) specify measuring the size of the weld nugget in terms of one or more welding variables, depending on the specification applied. The correlations of nugget size with current or with current and time are some of the most popular for qualification procedures. The importance of the current's influence on the soundness of the weld nugget has led to the development of welding lobes to define the current and time ranges where optimum spot welds can consistently be produced. However, this reproducibility is hampered by inconsistencies in metal composition, variation in surface finish and by electrode tip mushrooming.

The heat transfer model proposed defines the temperature of any location in the workpiece as a function of time from the start of the process. Consequently, it can also define the time when the weld nugget begins to form. Figure 9

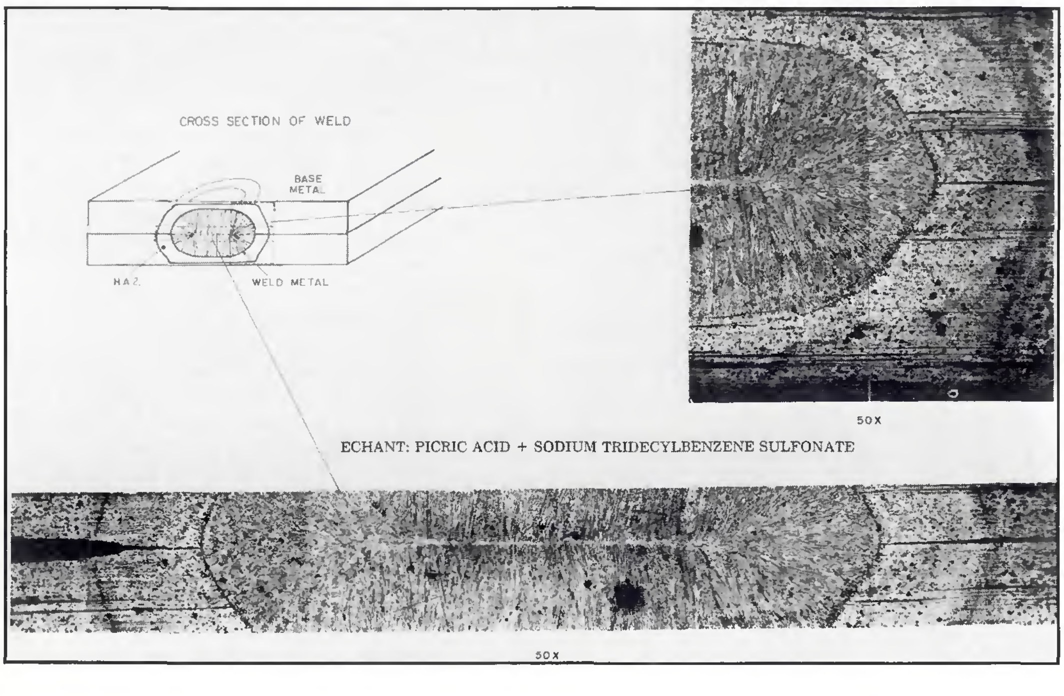

Fig. 8—Micrograph of a spot weld cross-section

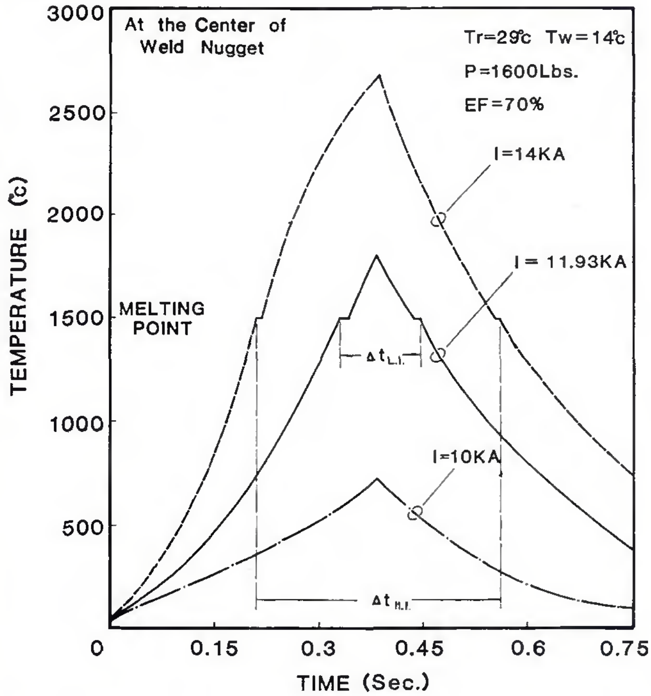

Fig. 9 — Theoretical temperature distributions as a function of time for three different currents

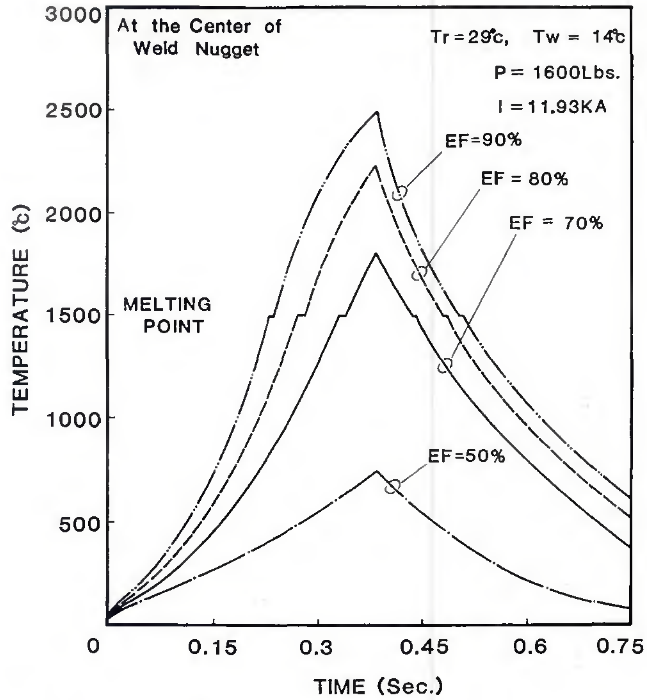

Fig. 10 — Theoretical temperature distributions as a function of time for different efficiencies

presents temperature versus time predictions at the center of the weld nugget at the faying surface. Computation of this information was done with the assumption of a fixed electrode force of 1600 lb and efficiency factor of 70%.

At low currents, undersize and brittle nuggets are formed because of the insufficient heat supplied to cause the asperity collapse and surface film breakdown. From the results observed in Fig. 9, it seems that a welding current of 14.0 kA will produce a larger nugget than 11.93 kA, since the supply of heat for the high current is larger not only because of the higher current, but also because of the time spent at melting temperature or above the melting point, as denoted by $\Delta t_{Low\ I}$ and $\Delta t_{High\ I}$. Correspondingly, the time to reach the melting temperature will be shorter for the high current than for the low current. The model predicts a time of 0.21 s for 14.0 kA versus 0.33 s for 11.93 kA, as seen in Fig. 9.

The welding efficiency factor is an important consideration in this model because of its effect on the accuracy of the model's predictions. Figure 10 reflects its significance. The use of an incorrect efficiency factor could either lengthen or shorten the period for start of nugget formation. The theoretical curves generated in Fig. 10 assume a constant electrode load of 1600 lb and current of 11.93 kA.

This heat transfer model has also been used to determine the heating and cooling rate as a function of time for any location in the workpiece (Appendix B). Figure 11 shows the heating and cooling rate curves superimposed with the temperature-time curve corresponding to the center of the weld nugget. Notice that the sudden drop in the heating rate corresponds to a constant temperature (melting point) of the workpiece (where the nugget would be formed) as a result of the heat absorption prior to melting. The time at which such drop occurs coincides with the time to reach the melting temperature as seen in Fig. 11.

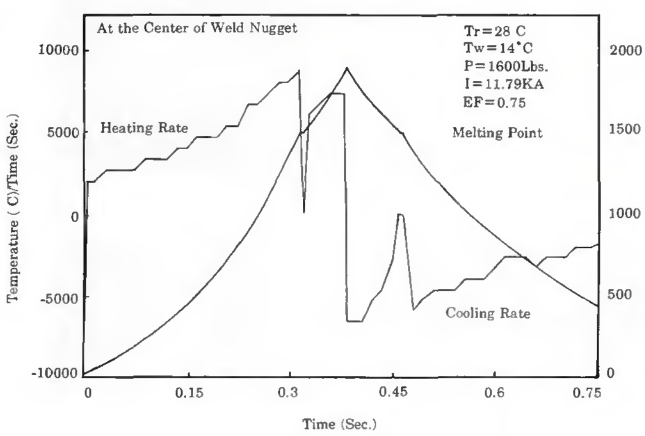

Fig. 11 — Theoretical temperature distributions and heating and cooling rates versus time at the weld center nugget

Effect of Electrode Force on Nugget Formation

In order to examine the effect of electrode force on the start of the nugget formation, temperature-time curves were calculated with this model using three different electrode forces — Fig. 12. All these curves correspond to a location at the center of the weld nugget and right at the faying interface.

As the electrode force was increased, the time to reach the melting temperature was delayed because of the general decrease in the resistance level. Such reduction in total resistance is expected because the increase in the applied pressure will decrease the thickness of the material between the electrodes and the contact area, primarily at the faying interface, will increase in view of the deformation of the asperities. Recall that the resistance is proportional to the length of the conductor and inversely proportional to the cross-sectional area ($R \alpha L/A$).

Since all the curves were calculated at the same current (11.93 kA and efficiency value 70%), decreasing resistance results in a decrease in the rate at which energy is supplied to the weld ($P = \eta I^2 R$). Thus the time to reach the temperature for melting is shifted to longer times and,

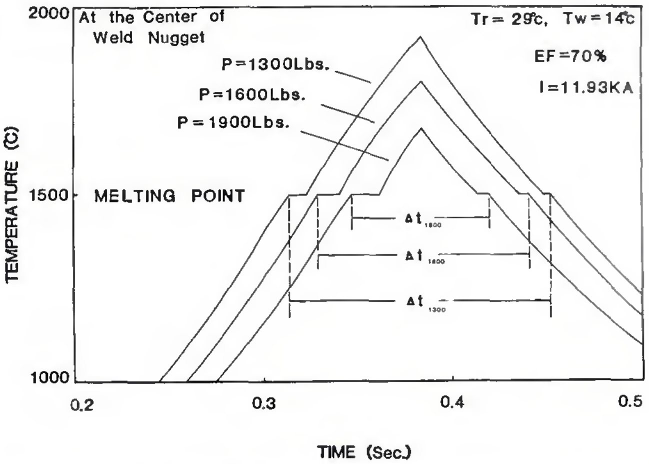

Fig. 12 — Theoretical temperature distributions as function of time for different electrode forces

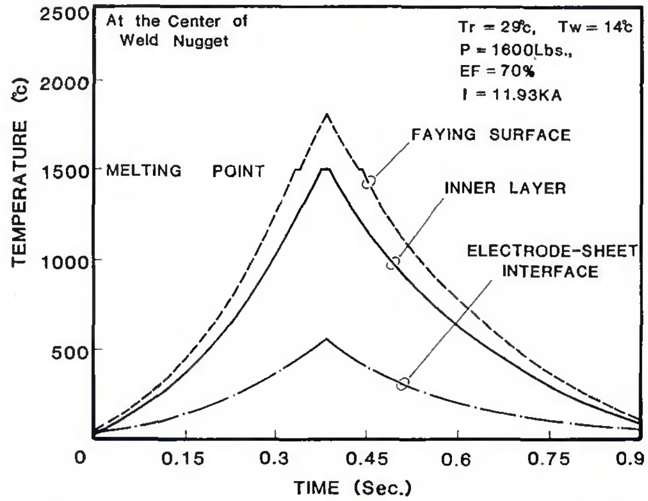

Fig. 13 — Predicted temperature distributions as a function of time at different positions from the faying interface along the electrode axis

consequently, nugget formation is delayed as electrode force is increased.

Lower electrode forces, therefore, should favor nugget formation and larger nugget size in view of the longer time and at or above the melting temperature for the same current, as observed in Fig. 12. At higher forces, the nuggets would be smaller, which could affect the ductility and soundness of the spot weld.

Correlations of Theoretical and Experimental Results

It has been indicated that this thermal model is capable of predicting the temperature as a function of time for any location in the workpiece. Figure 13 shows the peak temperatures reached along the vertical axis of the electrodes for different locations through the thickness of the sheet metal. Similar distribution of temperatures have been calculated along the faying interface at 1.0-mm (0.04-in.) steps from the electrode axis, as shown in Fig. 14.

A direct correlation between experimental and theoretical temperature-time curves is presented in Figs. 15 and 16. The thermocouple for the experimental curve was placed along the faying interface at a distance of 3.8 mm (0.15 in.) from the center of the weld nugget. Although the agreement is very reasonable, discrepancies were found primarily during the cooling cycle that could be attributed to some of the original assumptions made in the model's formulation. The selection of a relatively large grid size (1.0 mm) and the lack of an efficiency factor were some of the problems thought to be responsible for such deviations. Reduction in the mesh size and the step time, as well as the use of a higher efficiency factor (75%) improved the agreement between the experimental and theoretical curves, as shown in Figs. 15 and 16 for two different samples.

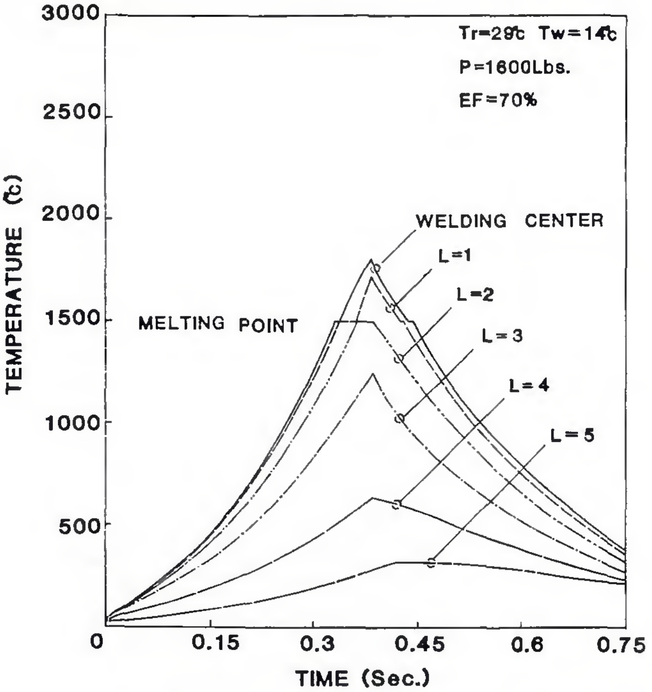

Fig. 14 — Predicted temperature distributions as a function of time in the workpiece for different points along the faying interface

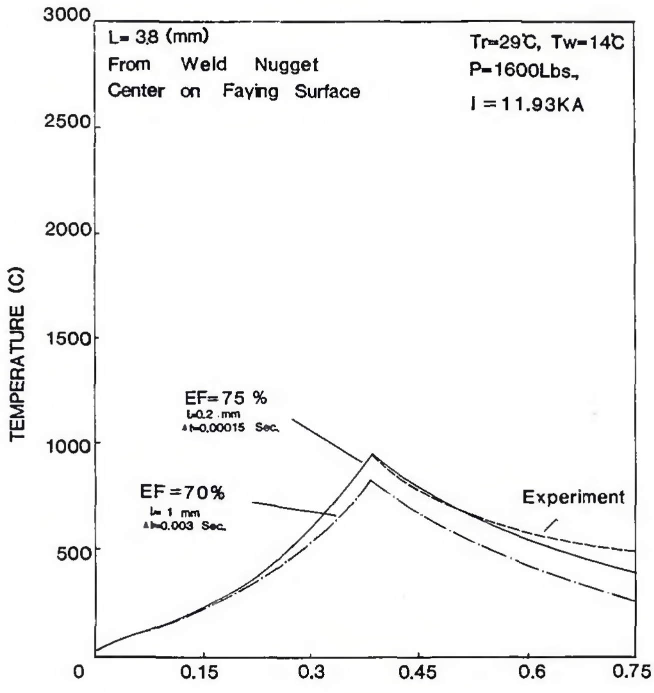

Fig. 15 — Comparison of theoretical and experimental temperature distributions for a point on the faying interface and 3.8 mm from the weld nugget centerline

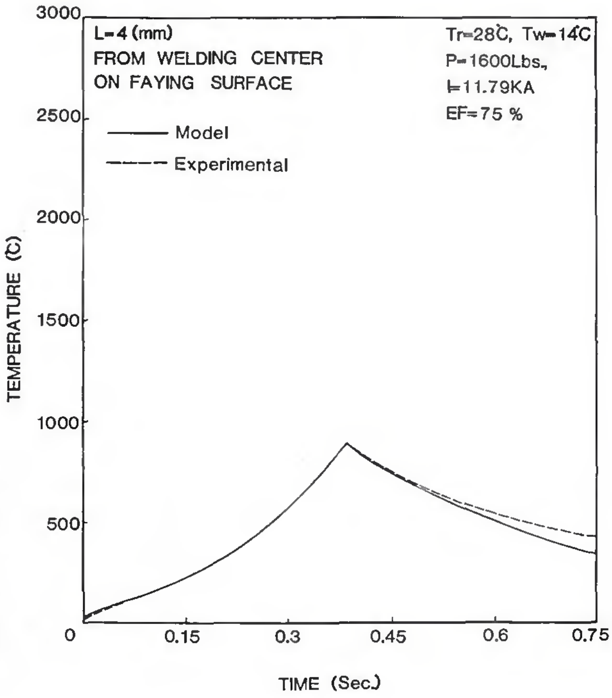

Fig. 16 — Comparison of theoretical and experimental temperature distributions for a point on the faying interface and 4.0 mm from the weld nugget centerline

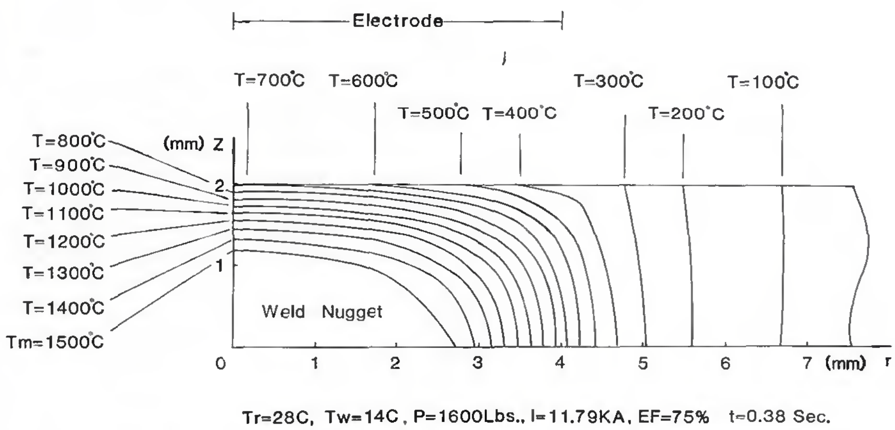

Fig. 17 — Predicted temperature profiles around the weld nugget and heat-affected zone of the spot weld

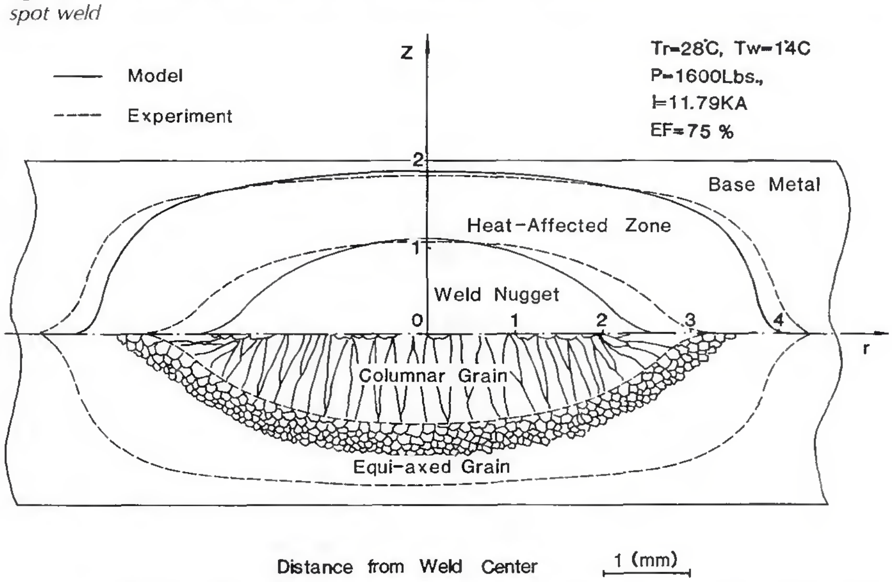

Fig. 18 — Schematic comparing the predicted and experimental weld nugget cross-section dimensions

The differences between the two curves are more noticeable during cooling and at the longer times, with the experimental curve having a slower cooling rate — Figs. 15 and 16. This is probably caused by the fact that material was removed to make a notch where the thermocouple was spot welded.

The model was used to map constant temperature curves for the spot weld at 0.38 s into the welding cycle, when the current was stopped at that instant. These curves were plotted for one of the quadrants of the spot welding system as shown in Fig. 17. The temperature distribution allows us to define the regions that underwent melting (weld nugget) and those that were affected by the heat of the process (HAZ). Based on this, the weld nugget size and HAZ were estimated, and these results have been schematically compared in Fig. 18 for a spot weld.

Conclusions

1) A finite difference thermal model was developed for resistance spot welding, capable of predicting the temperature as a function of time and location for any position in the workpiece, and for any low-carbon sheet steel. This model could also be applied to any other metal provided the physical properties of given material are included in the model.

2) Acceptable correlations between the theoretical and experimental temperatures have been made. The temperatures in the spot welds were measured using fine thermocouples imbedded in the sheet-steel coupons near the faying interface.

3) Improvement in the experimental techniques to monitor the thermal cycles, as well as the introduction of empirical data in the model should reduce the deviations that exist between the predicted and the experimental values.

4) This model can also predict indirectly the weld nugget size and the width of the HAZ. Work continues to improve the model to predict the microstructures and corresponding strengths of the HAZ.

Acknowledgments

The authors wish to acknowledge the financial support provided by Inland Steel Company for the work performed at the University of Illinois at Chicago. We are also grateful to Michael Bjornson for the extensive metallography and measurements performed on this project. Mr. Dan Galiher and Mr. Neal Saboff, who carried out the spot welds at Inland Steel Research Laboratories also are acknowledged. This project could have not been started without the tremendous support and encouragement from the late William Schumacher.

Appendix A

The Drop to Zero: an Explanation

The existence of a finite contact resistance is due principally to surface roughness effects. Heat transfer is therefore due to conduction across the actual contact area and to conduction (or natural convection) and radiation across the gaps. The contact resistance decreases with decreasing surface roughness. Since a more intimate contact is brought about

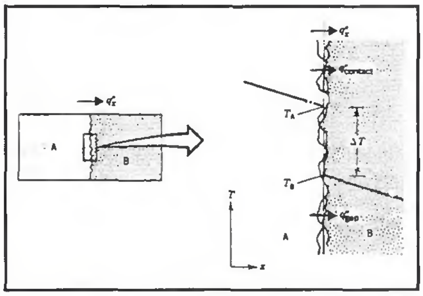

when melting occurs at the interface, it is reasonable to assume that the value of the contact resistance drops to zero. For additional information, the reviewer might consult *Fundamentals of Heat and Mass Transfer,* by Incropera and Dewitt, 2nd Edition, p. 67.

Appendix B

Based on the computer program developed, the time step $\Delta t^* = 0.00015$ s and mesh size $\ell = 0.2$ mm. The derivative of temperature with time for an instant n, at a location i, j, either for heating or cooling, can be defined as $dT/dt|_{i,j,n}$. This can be approximated as $\Delta T/\Delta t$ around the moment n, as shown in the following expression

$$\left.\frac{\Delta T}{\Delta t}\right|_{i,j,n} = \frac{T_{i,j,n+5} - T_{i,j,n-5}}{t_{i,j,n+5} - t_{i,j,n-5}} = \frac{T_{i,j,n+5} - T_{i,j,n-5}}{10 \times \Delta t^*} = \frac{T_{i,j,n+5} - T_{i,j,n-5}}{0.0015}$$

$\frac{\Delta T}{\Delta t} > 0$, in the heating stage

$\frac{\Delta T}{\Delta t} < 0$, in the cooling stage

$\frac{\Delta T}{\Delta t} = 0$, in the constant temperature of the melting temperature

References

1. *Ford Laboratory Test Methods,* Schedule BA 13-4, September 26, 1980.
2. *Fisher Body Weld Lobe Procedure,* December 1987.
3. Dickinson, D. W., Franklin, J. E., and Stanya, A. 1980. Characterization of spot welding behavior by dynamic electrical parameter monitoring. *Welding Journal* 59(6):170-s to 176-s.
4. Dickinson, D. W., and Natale, J. V. 1981. The effect of sheet surface on spot weldability. *Technological Impact of Surfaces,* ASM, Metals Park, Ohio, April 14-15.
5. *Spot Welding Sheet Steel,* AISI Technical Report, SG-936, 282-10RM-RI.
6. Gould, J. E. 1987. An examination of nugget development during spot welding, using both experimental and analytical techniques. *Welding Journal* 66(1):1-s to 10-s.
7. Goldak, J., Bibby, M., Moore, J., House, R., and Patel, B. 1986. Computer modeling of heat flow in welds. *Metallurgical Transactions B,* 17B(9):587.
8. Rice, W., and Funk, E. J. An analytical investigation of the temperature distributions during resistance welding. *Welding Journal* 46 (4):175-s to 186-s.
9. Krutz, G. W., and Segerlind, L. J. 1978. Finite element analysis of welded structures. *Welding Journal* 57 (7):211-s to 216-s.
10. Salcudean, M., Choi, M., and Greif, R. 1986. A study of heat transfer during arc welding. *Int. J. Heat Mass Transfer* 29 (2):215.
11. Nied, H. A. 1984. The finite element modeling of the resistance spot welding process. *Welding Journal* 63 (4):123-s to 132-s.
12. *Metals Handbook,* 8th Ed., ASM, Metals Park, Ohio, 6:408.
13. Bhattacharya, S., and Andrews, D. R. 1972. Resistance weld quality monitoring. *Sheet Metal Industries,* (7):400-466.
14. Roberts, W. L. 1951. Resistance variations during spot welding. *Welding Journal* 30(11):1004-1019.
15. Savage, W. F., Nippes, E. F., and Wassell, F. A. 1978. Dynamic contact resistance of series spot welds. *Welding Journal* 57 (2):43-s to 50-s.
16. Tipler, P. A. 1982. *Physics,* Worth Publishers, Inc., p. 675.
17. Ozisik, M. N. 1985. *Heat Transfer—A Basic Approach,* McGraw-Hill Book Company, p. 746.
18. Paley, Z., and Hibbert, P. D. 1975. Computation of temperatures in actual weld designs. *Welding Journal* 54 (11):385-s to 392-s.
19. Kaiser, J. G., Dunn, G. J., and Eagar, T. W. 1982. The effect of electrical resistance on nugget formation during spot welding. *Welding Journal* 61(6):167-s to 174-s.